Draft version June 9, 2023
Typeset using LaTeX **twocolumn** style in AASTeX631

arXiv:2202.01226v2 [astro-ph.GA] 7 Jun 2023

Updated void catalogs of the SDSS DR7 main sample

Kelly A. Douglass [1], Dahlia Veyrat [1], and Segev BenZvi [1]

[1] *Department of Physics & Astronomy, University of Rochester, 500 Wilson Blvd., Rochester, NY 14611*

ABSTRACT

We produce several public void catalogs using a volume-limited subsample of the Sloan Digital Sky Survey Data Release 7 (SDSS DR7). Using new implementations of three different void-finding algorithms, VoidFinder and two ZOBOV-based algorithms (VIDE and REVOLVER), we identify 1163, 531, and 518 cosmic voids with radii $> 10\,h^{-1}$ Mpc, respectively, out to a redshift of $z = 0.114$ assuming a Planck 2018 cosmology, and 1184, 535, and 519 cosmic voids assuming a WMAP5 cosmology. We compute effective radii and centers for all voids and find none with an effective radius $> 54\,h^{-1}$ Mpc. The median void effective radius is 15–19 h^{-1} Mpc for all three algorithms. We extract and discuss several properties of the void populations, including radial density profiles, the volume fraction of the catalog contained within voids, and the fraction of galaxies contained within voids. Using 64 mock galaxy catalogs created from the Horizon Run 4 N-body simulation, we compare simulated and observed void properties and find good agreement between the SDSS DR7 and mock catalog results.

1. INTRODUCTION

Galaxy redshift surveys have revealed a web-like distribution of galaxies in the observable universe (Bond et al. 1996). The cosmic web exhibits dense clusters connected by extended filaments separated by vast regions nearly empty of galaxies, known as voids. Rood (1988) reviewed the paradigm shift that started in the mid-1970s as galaxy redshift surveys began to develop in their depth, density, and sky coverage, enabling more detailed study of the three-dimensional spatial distribution of galaxies and the impact that this had on void studies. Early studies by Jõeveer et al. (1978), Gregory & Thompson (1978), and Kirshner et al. (1981) indicated the presence of large, underdense regions in the galaxy distribution, and the Center for Astrophysics Redshift Survey (Huchra et al. 1983) and its extension to $m_B = 15.5$ (de Lapparent et al. 1986; Geller & Huchra 1989) revealed that voids dominate the large-scale structure of the universe. The voids likely evolved from primordial underdensities in the early universe and are a ubiquitous feature of gravitational instabilities and the growth of structure (van de Weygaert & Platen 2011, and references therein).

Because voids possess much lower densities relative to clusters and filaments, their gravitational evolution remains in the linear regime through much of their formation, and at later times they become dominated by dark energy earlier than other regions of the universe (Goldberg & Vogeley 2004). As discussed in the review by van de Weygaert & Platen (2011), the unique properties of void environments make them important probes of cosmology and galaxy formation. For example, voids have been used in Alcock-Paczyński tests (Lavaux & Wandelt 2012; Sutter et al. 2012a, 2014b; Hamaus et al. 2016; Mao et al. 2017; Nadathur et al. 2019; Hamaus et al. 2020), to constrain the dark energy equation of state (e.g., Lavaux & Wandelt 2012; Pisani et al. 2015; Verza et al. 2019), and to measure the scale of baryon acoustic oscillations (e.g., Kitaura et al. 2016; Liang et al. 2016; Nadathur et al. 2019; Zhao et al. 2020, 2021). In addition, galaxies are known to evolve differently in voids compared to galaxies in denser environments, collapsing earlier and forming stars later.

Searches for voids in the distribution of galaxies have historically been based on one of two strategies: either by locating relatively empty spherical regions in the galaxy distribution, or using a watershed algorithm to

Corresponding author: Kelly A. Douglass
kellyadouglass@rochester.edu

dveyrat@ur.rochester.edu

segev.benzvi@rochester.edu

link low-density regions. The most widely-used void catalogs produced to date are based on the 7th data release of the Sloan Digital Sky Survey (SDSS DR7; Abazajian et al. 2009), which is complete to a Petrosian r-band magnitude $m_r = 17.77$. The first SDSS DR7 void catalog, published by Pan et al. (2012), was constructed from a union of relatively empty spheres and has been used to study void structure (Alpaslan et al. 2014; Lee & Hoyle 2015; Shim et al. 2015), the properties of galaxies in voids (Hoyle et al. 2012; Moorman et al. 2014, 2015; Liu et al. 2015; Penny et al. 2015; Fraser-McKelvie et al. 2016; Moorman et al. 2016; Douglass & Vogeley 2017a,b; Douglass et al. 2018, 2019; Miraghaei 2020), the intergalactic medium in voids (Tejos et al. 2012), and for cosmological analyses (Ilić et al. 2013; Planck Collaboration et al. 2014). The void catalog of Sutter et al. (2012b) is based on the watershed algorithm and has been used to study the properties of void galaxies (Furniss et al. 2015; Trevisan et al. 2021) and for cosmological analyses (Sutter et al. 2012a; Ilić et al. 2013; Hamaus et al. 2014b; Sutter et al. 2014b; Pisani et al. 2014; Planck Collaboration et al. 2014; Cai et al. 2014; Melchior et al. 2014; Chen et al. 2015; Dai 2015; Chantavat et al. 2017).

In this work, we present updated void catalogs based on the SDSS DR7 galaxy sample from the NASA-Sloan Atlas (NSA; Blanton et al. 2011). We have generated catalogs using the two main void-finding algorithms, which have been implemented in the Void Analysis Software Toolkit (VAST; Douglass et al. 2022). These implementations include improved handling of survey boundaries and increased computational efficiency for void finding. This is the first time that void catalogs have been generated using complementary algorithms on the same volume-limited[1] galaxy survey. We use the SDSS DR7 catalog because it remains the most complete galaxy catalog of the nearby universe produced to date.

The paper is structured as follows. In Section 2 we describe the SDSS DR7 data sample, the cuts used to produce a volume-limited catalog, and the simulation used to produce mock catalogs. We describe the void-finding algorithms in Section 3 and the resulting void catalogs in Section 4. In Section 5, we compare our catalogs with previous results.

2. DATA AND SIMULATIONS

2.1. *Data: SDSS DR7*

Released in 2009, the SDSS DR7 (Abazajian et al. 2009) is a wide-field multiband imaging and spectroscopic survey conducted on the 2.5 m telescope at the Apache Point Observatory in New Mexico. Photometric data in the SDSS five-band system (Fukugita et al. 1996; Gunn et al. 1998) was collected using a drift scanning technique to image approximately one quarter of the night sky. Follow-up spectroscopy was performed on all galaxies with a Petrosian r-band magnitude $m_r < 17.77$ (Lupton et al. 2001; Strauss et al. 2002) with two double fiber-fed spectrometers and fiber plug plates with a minimum fiber separation of 55". The observed wavelength range for the SDSS DR7 spectra is 3800–9200Å with a resolution $\lambda/\Delta\lambda \sim 1800$ (Blanton et al. 2003).

We use version 1.0.1 of the NASA-Sloan Atlas (NSA; Blanton et al. 2011), which contains 641,409 galaxies observed in SDSS DR7. We construct a volume-limited sample from the NSA by requiring all objects to have an absolute r-band magnitude $M_r \leq -20$ and redshift $z \leq 0.114$. This is necessary to remove the natural decrease in matter tracer density with increasing redshift present in magnitude-limited surveys, as this would introduce an artificial relationship between void radius and redshift. Our luminosity limit is selected to retain all galaxies brighter than L_*, which have been shown to sufficiently trace the cosmic web structure (Pan et al. 2012). The redshift limit corresponds to the distance at which these $M_r = -20$ objects are spectroscopically observed by SDSS DR7. Within the main SDSS DR7 footprint, 194,125 galaxies are in the volume-limited sample.

2.2. *Mock Catalogs: Horizon Run 4 Simulations*

We create 64 mock galaxy catalogs generated from the Horizon Run 4 Simulation (Kim et al. 2015) to estimate the variances of the void spectra and density profiles. Horizon Run 4 is an N-body simulation generated from 6300^3 particles in a cubic box with side length 3150 h^{-1} Mpc using the WMAP 5-year ΛCDM cosmology: $\Omega_m = 0.258$, $\Omega_\Lambda = 0.742$, $h = 0.719$, $\sigma_8 = 0.796$, and $n_s = 0.963$ (Dunkley et al. 2009). As part of Horizon Run 4, Hong et al. (2016) produced a mock galaxy catalog, calibrating it to match the properties of galaxy groups in volume-limited SDSS galaxy catalogs. The resulting mock catalog is divided into 64 cubic equal-volume subsamples.

To replicate the angular and redshift distribution of galaxies in SDSS DR7, we create a mock catalog from each Horizon Run 4 subsample by applying cuts in right ascension, declination, and redshift relative to an observer positioned at the center of the cubic volume. Further, the mock galaxy catalogs provide a mass-like quantity computed from the friends-of-friends halo mass

[1] Previous void catalogs produced in SDSS DR7 did not use the same volume-limited sample.

(Hong et al. 2016), which can be used as a proxy for luminosity. By applying a cut on this quantity, we match the redshift selection function of the volume-limited SDSS DR7 catalog in each of the 64 mocks.

3. THE VOID ANALYSIS SOFTWARE TOOLKIT

We construct voids using the Void Analysis Software Toolkit[2] (VAST; Douglass et al. 2022). VAST provides Python-only implementations of two popular classes of void-finding algorithms: VoidFinder, which identifies voids by growing and merging nearly empty spherical regions in a galaxy catalog; and V^2, which uses a watershed algorithm to link low-density cells in a Voronoi tesselation of the galaxy catalog.

3.1. *VoidFinder*

Originally described by El-Ad & Piran (1997) and implemented by Hoyle & Vogeley (2002), VoidFinder identifies apparent dynamically distinct voids by growing empty spheres within a galaxy distribution and then merging the spheres to form voids. VoidFinder first locates and removes all isolated, or field, galaxies, defined by the distance to their third-nearest neighbor, and then places the remaining non-isolated, or wall, galaxies on a 3D grid. A sphere is then grown from each empty cell in the grid until it is bounded by four galaxies. To keep voids from extending beyond the survey edges, a sphere is removed if more than 10% of its volume lies outside of the survey.

To extract apparent dynamically-distinct voids from the resulting list of spheres, the spheres are sorted by radius, and the largest is identified as a maximal sphere — the largest sphere that can fit inside a given void region. Each subsequent sphere with a radius larger than 10 h^{-1} Mpc is also labeled as a maximal sphere if it does not overlap any already-identified maximal sphere by more than 10% of its volume. To refine the volume and profile of the void regions, all spheres not identified as maximal spheres are merged with a maximal sphere if they overlap exactly one maximal sphere by at least 50% of their volume. A void is therefore defined as a union of spheres: one maximal sphere, plus some number of smaller spheres.

3.2. *Voronoi Voids (V^2)*

Voronoi Voids, or V^2, is a Python-only implementation based on the ZOBOV algorithm (Neyrinck 2008). It first produces a 3D Voronoi tessellation of the input catalog to separate each galaxy into a primitive cell. Each cell's volume is computed and used to estimate the local density in 3D. The Voronoi cells are subsequently combined into groups or "zones" using watershed segmentation. Each cell is put into the same zone as its least-dense neighbor, and any cell less dense than any of its neighboring cells — a local density minimum — is identified as its zone's central cell.

Zones are merged to form voids by first identifying the least-dense pair of adjacent cells between two zones. The set of all zones is partitioned into a subset of voids linked together by zones of equal or lower density, called the "linking density." The algorithm loops over linking density values to produce the voids. Because this zone-linking procedure produces a hierarchy of voids ranging from individual small zones to one huge void encompassing the survey volume, a pruning step is used to fix the final number of voids. This can proceed either by setting a user-defined maximum zone linking density (VIDE pruning; Sutter et al. 2015), or by estimating the probability that any given void is due to catalog shot noise and removing the voids most likely produced by shot noise (ZOBOV pruning; Neyrinck 2008). Alternatively, one can simply define voids as single zones with volume above some threshold, such as the median volume of all zones (REVOLVER pruning; Nadathur et al. 2019, similar to VIDE pruning with an arbitrarily small zone-linking density and a minimum radius cut). The density threshold for a given pruning method can also be determined by computing the effective radius of an equivalent spherical void,

$$R_{\rm eff} = \left(\frac{3V}{4\pi}\right)^{1/3} \tag{1}$$

where V is the void volume, and then selecting $R_{\rm eff}$ greater than some user-defined threshold. To compute the center of each void, V^2 uses a sum over the positions of the constituent galaxies, weighted according to their Voronoi volumes.

The use of a Voronoi tessellation assigns arbitrarily large volumes to cells near the boundary of the survey, impacting the calculation $R_{\rm eff}$ in Eqn. (1). To account for this effect, V^2 assigns a volume of 0 to any cell that extends outside the edge of a survey. Effectively, the edge is treated as an infinitely dense wall surrounding the survey through which zones cannot penetrate.

4. SDSS DR7 VOID CATALOGS

We present void catalogs found with VoidFinder, V^2 with VIDE pruning (V^2/VIDE), and V^2 with REVOLVER pruning (V^2/REVOLVER) assuming two flat ΛCDM cosmologies: WMAP5 ($\Omega_M = 0.258$; Dunkley et al. 2009) and Planck 2018 ($\Omega_M = 0.315$;

[2] VAST is available for download at https://github.com/desi-ur/vast.

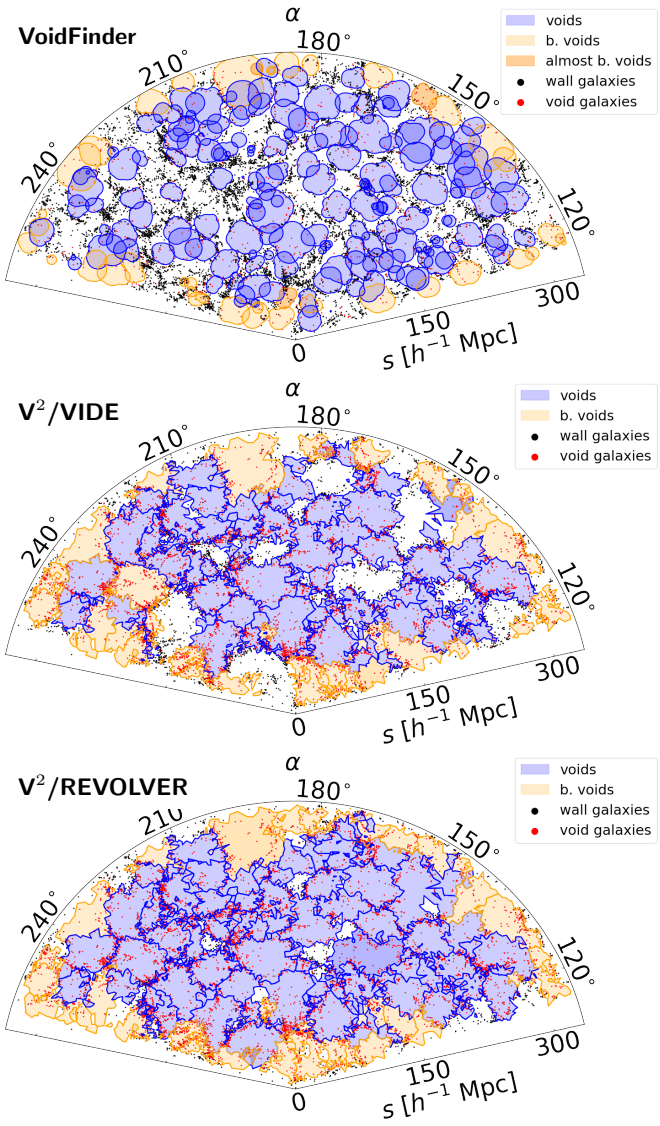


Figure 1. A 10 h^{-1} Mpc thick slice of SDSS DR7 centered at a declination of 25 deg assuming Planck 2018 cosmology. The locations of the galaxies which fall within a void are shown in red, while those which do not are shown in black. The intersection of all voids with the center of this slice are shown in the shaded blue (orange for boundary voids) regions, for VoidFinder (top), V^2/VIDE (middle), and V^2/REVOLVER (bottom).

Planck Collaboration et al. 2020), and assuming $H_0 = 100h$ km/s/Mpc. Each void-finding algorithm produces a different void catalog for the same volume-limited galaxy sample. Examples of the void locations relative to the galaxies are shown in Figure 1 for VoidFinder (top), V^2/VIDE (middle), and V^2/REVOLVER (bottom). The galaxies that fall within a void region defined by the corresponding void catalog are colored in red, while those that do not are shown in black. The three void catalogs identify approximately the same regions as voids, but the details of their borders, including exactly where the void ends, is very different between VoidFinder and V^2. The effect that this has on the inferred properties of void galaxies is discussed in Zaidouni et al. (in prep.).

Our void catalogs are publicly available at https://doi.org/10.5281/zenodo.5834786. Both algorithms produce output files in `ASCII` format. The file contents are different due to the differences in the void-finding algorithms and are described below.

The VoidFinder void catalog consists of two files, one containing the maximal spheres and the other containing a list of all of the spheres that are part of a void. The maximal sphere file contains the coordinates of the centers of the maximal spheres (in both Cartesian and sky coordinates), along with their radii, unique identifiers, the effective radii of the voids, and whether the void sits close to the edge of the survey. We use the following transformations to convert from sky coordinates (α, δ) to Cartesian coordinates:

$$x = s\cos(\alpha)\cos(\delta) \quad (2)$$

$$y = s\sin(\alpha)\cos(\delta) \quad (3)$$

$$z = s\sin(\delta) \quad (4)$$

where s is the comoving distance to the galaxy using one of the two flat ΛCDM cosmologies specified earlier. The first few lines of this file are shown in Table 1. The file listing all of the spheres (including the maximal spheres) contains each sphere's center in Cartesian coordinates, its radius, and the unique identifier corresponding to its void's maximal sphere. A portion of this file can be found in Table 2. The union of all spheres with the same unique identifier define one void.

We provide two V^2 void catalogs, one with VIDE pruning (maximum zone linking density of $0.2\overline{n}$, as described in Sutter et al. 2015) and a minimum $R_{\rm eff}$ of 10 h^{-1} Mpc, and the other with REVOLVER pruning. The minimum radius limit for the V^2/VIDE catalog is chosen to closely match the minimum maximal sphere radius of 10 h^{-1} Mpc in VoidFinder's void catalog. Each of the V^2 void catalogs consists of three files, one containing the details of the voids, one describing the connection between the zones and voids, and one describing the connection between the galaxies and zones. The void file contains the Cartesian coordinates, redshift, and sky coordinates of each void's volume-weighted center[3], along with each void's effective radius (Eqn. 1), the

[3] The volume-weighted center the average position of all galaxies in the voids, weighted by the Voronoi volume of each galaxy.

Table 1. VoidFinder output: Maximal spheres

x	y	z	radius	flag	edge	s	ra	dec	Reff
h^{-1} Mpc	h^{-1} Mpc	h^{-1} Mpc	h^{-1} Mpc			h^{-1} Mpc	deg	deg	h^{-1} Mpc
(1)	(2)	(3)	(4)	(5)	(6)	(7)	(8)	(9)	(10)
−169.041	162.884	209.440	22.441	0	1	314.597	136.062	41.739	27.855
−135.968	52.528	271.538	22.335	1	1	308.187	158.877	61.772	30.611
−167.611	95.791	251.200	21.814	2	1	316.814	150.251	52.456	27.942
−269.456	−80.652	134.977	21.761	3	1	311.978	196.663	25.635	29.541
−229.344	110.975	103.677	21.144	4	0	275.069	154.178	22.142	28.694

NOTE—Five of the 1163 maximal spheres of the VoidFinder SDSS DR7 void catalog assuming a Planck 2018 cosmology. This table is published in its entirety online in a machine-readable format. A portion is shown here for guidance regarding its form and content. Columns include: (1–3) Cartesian coordinates of maximal sphere center; (4) Radius of maximal sphere; (5) Unique identifier; (6) Flag identifying whether any part of the void falls outside of the survey mask; (7) Comoving distance of maximal sphere center; (8–9) Sky coordinates of maximal sphere center; (10) Effective radius of the void to which the maximal sphere belongs.

Table 2. VoidFinder output: All spheres

x	y	z	radius	flag
h^{-1} Mpc	h^{-1} Mpc	h^{-1} Mpc	h^{-1} Mpc	
(1)	(2)	(3)	(4)	(5)
−169.041	162.884	209.440	22.441	0
−169.267	163.627	210.224	22.362	0
−135.968	52.528	271.538	22.335	1
−169.634	162.112	207.992	22.291	0
−136.764	52.442	271.932	22.233	1

NOTE—Five of the 39,735 spheres in the VoidFinder SDSS DR7 void catalog assuming a Planck 2018 cosmology. This table is published in its entirety online in a machine-readable format. A portion is shown here for guidance regarding its form and content. Columns include: (1–3) Cartesian coordinates of sphere center; (4) Radius of sphere; (5) Unique identifier. The union of all spheres with the same unique identifier form one void.

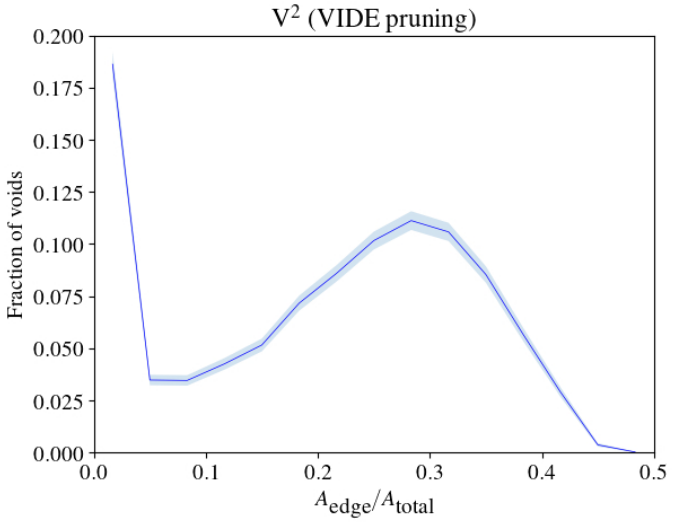


Figure 2. Distribution of the ratio of the surface area of V^2 voids shared with boundary cells (A_{edge}) to the total surface area of each void (A_{total}), for all voids with $A_{edge} > 0$.

principal axes of the ellipsoid fitted to each void, the total surface area of the void, and the surface area of the void shared with a boundary galaxy cell. The zone file contains each zone's unique identifier, the smallest void to which it belongs, and the largest void to which it belongs. The galaxy file contains each galaxy's unique identifier (from the input galaxy catalog), the zone to which it belongs, the number of adjacent cells between its Voronoi cell and the edge of the zone to which it belongs, and flags to identify whether it is at the edge of or outside the survey mask. Excerpts from these files are shown in Tables 3–5.

4.1. *Defining boundary voids*

Voids found along the edges of the galaxy survey can be subject to boundary effects, as there is no information for which the voids can be constrained beyond the survey boundary. For each void in all catalogs, we include information to indicate if the void is potentially

affected by the finite volume of the survey, so that the user can easily filter these out if their analysis is sensitive to these boundary conditions.

In the case of VoidFinder, we define boundary voids as those with any part of their surface extending beyond the survey mask. These voids are flagged with a value of 1 in the `edge` column of the maximal spheres file. In our SDSS DR7 void catalog presented here, this includes 383 voids, or ∼33% of the voids in the catalog. These voids are shown in orange in the top panel of Figure 1. We also identify voids that have at least one sphere with a center within $10h^{-1}$ Mpc of the survey mask; these are flagged with a value of 2 in the `edge` column.

For V^2, we define boundary voids as those with a significant fraction of their surface area shared with a boundary galaxy's Voronoi cell (described in Sec. 3.2. Included in the V^2 void files are columns containing the total surface area of the voids and the surface area of the voids shared with these boundary cells. To determine which V^2 voids are significantly impacted by the survey bounds, we examine the distribution of the ratio of the surface area of V^2 voids shared with boundary cells, $A_{\rm edge}$, to the total surface area of each void, $A_{\rm total}$. As shown in Fig. 2, we find two distinct populations in the distribution between voids with surface area shared with boundary cells less than and greater than ∼10% of the total surface area of the void. For studies that are sensitive to an inaccurate $R_{\rm eff}$ (e.g., the void spectrum) shown below, we exclude voids with $A_{\rm edge}/A_{\rm total} > 0.1$; this includes 234 voids (∼44%) in the V^2/VIDE and 216 voids (∼42%) in the V^2/REVOLVER SDSS DR7 void catalogs. These voids are shown in orange in Figure 1. We include the areas in the catalogs so that the user has the freedom to be as restrictive as they find necessary for their analysis.

4.2. *Properties of the void catalogs*

We find 1163 voids in SDSS DR7 with VoidFinder, 531 voids with V^2/VIDE, and 518 voids with V^2/REVOLVER assuming Planck 2018 cosmology, and 1184, 534, and 518 voids assuming WMAP5 cosmology, respectively. The voids found by VoidFinder have a median effective radius $R_{\rm eff} = 15.5 \pm 0.1\ h^{-1}$ Mpc, and contain ∼61% of the survey volume and ∼18% of the galaxies in the volume-limited DR7 catalog. (The survey volume contained within voids is estimated by counting up the fraction of test particles placed on a $1\ h^{-1}$ Mpc grid that fall within one of the VoidFinder void spheres.) With V^2/VIDE, voids have a median $R_{\rm eff} \simeq 17\ h^{-1}$ Mpc ($\simeq 19.5\ h^{-1}$ Mpc in the case of V^2/REVOLVER), and contain 63–68% (86–90%) of the survey volume and ∼64% (∼82%) of the volume-limited

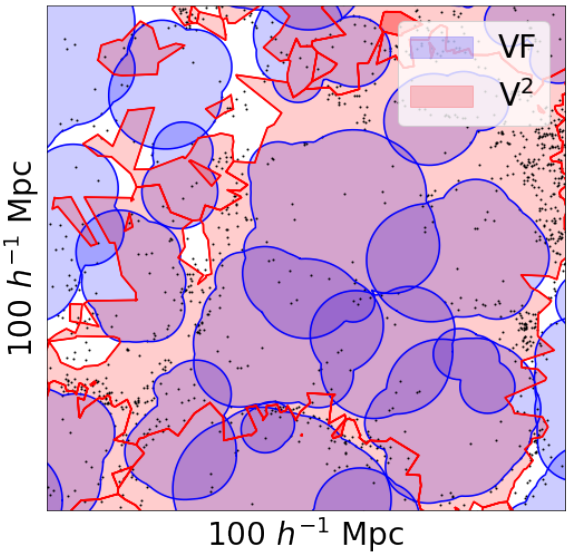


Figure 3. Example volume overlap between two void catalogs: VoidFinder (blue) and V^2 (red). Within the survey volume, we calculate the fraction of the space that both catalogs classify as a void (purple).

galaxies. While all three algorithms resulted in similar median effective radii, the $R_{\rm eff}$ of the largest void differs significantly, ranging from 28.7 h^{-1} Mpc with VoidFinder to 53.3 h^{-1} Mpc with V^2/VIDE. The catalog statistics are summarized in Table 6.

There is a significant difference in the fraction of galaxies contained within voids found by VoidFinder and voids found by V^2. While the void-growing step in VoidFinder explicitly stops once wall galaxies are encountered, V^2 voids extend to the peaks of the density maxima surrounding them. Thus, many galaxies in overdense regions are incorrectly classified as void galaxies by V^2, as can be seen by the significant fraction of void galaxies in extremely dense regions of the galaxy distribution shown in the middle and lower panels of Figure 1. V^2 is not ideal for isolating the void environment, a crucial detail for void-galaxy classification (Florez et al. 2021, Zaidouni et al., in prep.). However, V^2 is useful for studying galaxy properties as a function of large-scale environment by using the volumes of the Voronoi cells as a proxy for local density (e.g., Goh et al. 2019; Habouzit et al. 2020; Paranjape & Alam 2020; Jamieson & Loverde 2021).

Because VoidFinder and V^2 define voids differently, we study their application to the survey volume so that we can quantitatively compare their void catalogs. As demonstrated in Figure 3, we compute the percentage

Table 3. V^2 output: Voids

x	y	z	redshift	ra	dec	radius	x1 ...	x2 ...	x3 ...	area	edge
h^{-1} Mpc	h^{-1} Mpc	h^{-1} Mpc		deg	deg	h^{-1} Mpc	h^{-1} Mpc	h^{-1} Mpc	h^{-1} Mpc	$(h^{-1}$ Mpc$)^2$	$(h^{-1}$ Mpc$)^2$
(1)	(2)	(3)	(4)	(5)	(6)	(7)	(8–10)	(11–13)	(14–16)	(17)	(18)
−133.845	80.947	256.018	0.102	148.835	58.576	23.904	−4.244	25.889	−21.679	20096.9	2010.5
−245.112	134.208	113.007	0.103	151.297	22.018	26.164	−8.689	22.479	−6.785	25769.4	1736.4
−134.931	27.948	261.080	0.100	168.297	62.175	22.857	−4.066	24.292	21.974	18592.4	2719.4
−246.946	−59.461	82.552	0.091	193.538	18.004	24.167	−10.082	−13.396	−0.247	20203.4	0.0
−220.533	184.126	89.876	0.102	140.140	17.371	23.049	6.221	−23.418	−11.415	17058.4	1160.7

NOTE—Five of the 531 voids in the V^2/VIDE SDSS DR7 void catalog assuming a Planck 2018 cosmology. This table is published in its entirety online in a machine-readable format; a portion is shown here for guidance regarding its form and content. Columns include: (1–3) Cartesian coordinates of the void's weighted center; (4) Redshift of the void's weighted center; (5–6) Sky coordinates of the void's weighted center; (7) Effective radius of the void; (8–10) Cartesian components of the void's first ellipsoid axis (only x-value is shown); (11–13) Cartesian components of the void's second ellipsoid axis (only x-value is shown); (14–16) Cartesian components of the void's third ellipsoid axis (only x-value is shown); (17) Total surface area of the void; (18) Surface area of the void which is adjacent to boundary cells.

Table 4. V^2 output: Zones

zone	void0	void1
(1)	(2)	(3)
0	-1	-1
1	-1	-1
2	-1	-1
3	96	96
4	-1	-1

NOTE—Five of the 1037 zones in the V^2/VIDE SDSS DR7 void catalog assuming a Planck 2018 cosmology. This table is published in its entirety online in a machine-readable format; a portion is shown here for guidance regarding its form and content. Columns include: (1) Unique zone identifier; (2) Unique identifier of the smallest void to which the zone belongs; (3) Unique identifier of the largest void to which the zone belongs. A void's unique identifier is equal to its row number in the file described in Table 3. Values of -1 indicate that the zone is not part of any void.

Table 5. V^2 output: Galaxies

gal	zone	depth	edge	out
(1)	(2)	(3)	(4)	(5)
3	1036	0	1	0
7	1036	0	1	0
10	433	3	0	0
12	1036	0	1	0
13	1036	0	1	0

NOTE—Five of the 194,125 galaxies in the volume-limited SDSS DR7 catalog with void information corresponding to the V^2/VIDE void catalog assuming a Planck 2018 cosmology. This table is published in its entirety online in a machine-readable format; a portion is shown here for guidance regarding its form and content. Columns include: (1) Galaxy unique identifier (taken from the input catalog when possible); (2) Unique identifier for the zone to which the galaxy belongs; (3) Number of adjacent Voronoi cells between the galaxy's Voronoi cell and the edge of the zone to which it belongs; (4) Boolean value determining whether or not the galaxy is at the edge of the survey mask; (5) Boolean value determining whether or not the galaxy is outside the survey mask.

of the survey volume that two catalogs both consider to be a void (shaded in purple in Figure 3), and we compute the percentage of the volume-limited galaxy catalog that two algorithms both classify to be void galaxies. In other words, for any two void catalogs A and B, we compute the volume of $A \cap B$ and report the fraction of the survey inside the volume $A \cap B$. We also compute the percentage of galaxies inside the volume $A \cap B$. If the fractional survey volume in voids in catalog A from Table 6 is close to the fractional volume in voids in $A \cap B$ (Table 7), it implies that the void volume in catalog B contains most of the void volume in catalog A.

For example, consider V^2/REVOLVER. The fractional survey volumes in voids for V^2/REVOLVER ∩ VoidFinder and V^2/REVOLVER ∩ VIDE are within a few percent of the fractional survey volumes identified as voids with VoidFinder and V^2/VIDE alone. This is unsurprising: since V^2/REVOLVER identifies ∼90% of the survey volume to be within voids, the V^2/REVOLVER voids tend to contain the voids identified by VoidFinder and/or V^2/VIDE. These overlaps can also be seen in Figure 1, where it is visually clear that the V^2/REVOLVER voids (red areas) tend to contain the VoidFinder voids (blue areas).

In contrast, the percent survey volume identified commonly as void regions with both VoidFinder and V^2/VIDE (∼40%) reveals significant differences between these two catalogs. VoidFinder identifies ∼61% of the survey volume as a void, indicating that ∼20% of the survey volume identified as void by VoidFinder is classified as wall by V^2/VIDE. This can be seen in Figure 1, where there are apparent underdense regions classified as a void by VoidFinder but not included in either V^2 catalog.

For comparison, we also compute the fraction of void volume overlap and void galaxy overlap using the 64 mock catalogs and report them at the bottom of Tables 6 and 7. Overall there is good agreement with data, which tend to have slightly fewer voids than the mocks. The large variation in maximum $R_{\rm eff}$ for V^2/VIDE is likely a manifestation of the large relative uncertainty in the frequency of the zone-linking process that produces the largest voids in the catalog.

4.3. *Void spectrum*

The distributions of void effective radii are shown in Figure 4 for VoidFinder (left), V^2/VIDE (middle), and V^2/REVOLVER (right). Boundary voids, as defined in Sec. 4.1, are excluded from these spectra, as their radii are likely affected by the finite volume of SDSS DR7. Because the maximal spheres in VoidFinder are limited to a 10 h^{-1} Mpc minimum radius as opposed to the 10 h^{-1} Mpc minimum effective radius cut on the V^2/VIDE, the peak in the void spectrum for VoidFinder occurs at a larger radius than 10 h^{-1} Mpc. Additionally, the VoidFinder distribution drops off at ∼30 h^{-1} Mpc, while for the V^2 algorithms this occurs at 40–50 h^{-1} Mpc. This is a result of VoidFinder identifying apparent dynamically distinct voids, which evolve independently and are smaller and more numerous than the voids found by V^2.

Our distributions of the void effective radii agree reasonably well with the catalogs of Pan et al. (2012) and Sutter et al. (2012b). The most significant differences occur between our VoidFinder catalog and that of Pan et al. (2012) and are a result of our improved treatment of the survey boundaries and sphere merging in our implementation of VoidFinder (see Section 5 for details).

4.4. *Void density profile*

Gravitational theory predicts that void boundaries form from shell crossing, where the void interior expands faster than the collapsing denser regions (Sheth & van de Weygaert 2004). As a result, we expect voids to be surrounded by regions of higher density than average. While voids tend to exhibit an underdensity of galaxies near their centers, the radial density profiles of individual voids vary considerably within the population. For this reason, it is useful to define a stacked void density profile, where the density n in each radial bin is computed from a sum over all voids of the number of galaxies in that bin normalized by the volume of that bin that is within the survey. The spherically averaged stacked density profile $\delta(r)$ is then defined as

$$\delta(r) = \frac{n(r)}{\bar{n}} - 1, \tag{5}$$

where $\bar{n}$ is the average density of the survey.

The distribution over $1 + \delta(r)$ is shown in Figure 5 for the VoidFinder (top left), V^2 using V^2/VIDE (top right), and V^2/REVOLVER (bottom left) SDSS DR7 void catalogs. As expected, the density profiles exhibit the expected behavior of approaching 1 at large r.

Due to the range of void sizes in the population, the overdense wall feature in the density profiles of smaller voids can overlap with the underdense central regions of larger voids, resulting in a smearing of the wall feature in the void density profile. To counteract this effect, we compute a normalized stacked void density profile, where the radial bins are scaled in relation to each void's effective radius; the resulting density profiles are shown in Figure 6. There is a clear enhancement in the strength of the central underdensity relative to the wall feature, particularly for the void catalogs of VoidFinder and V^2/REVOLVER.

For each of our void catalogs, we find that the mock galaxy catalogs exhibit an overdensity in the voids relative to that observed in SDSS DR7. This indicates that the Horizon Run 4 simulations either use a different galaxy bias than exists in the data or produce a matter distribution whose underdense regions are not as underdense as the observed galaxy distribution. If either of these are the case, then the mock voids are less empty than the observed voids, so we would expect the VoidFinder algorithm to grow slightly smaller voids than in data, and to observe slightly more void galaxies in the

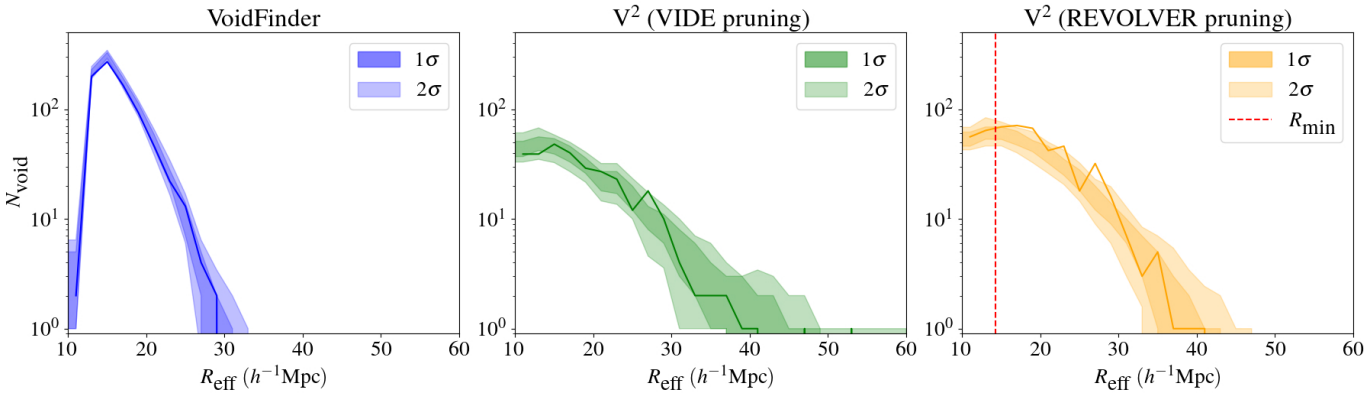


Figure 4. Distribution of voids' effective radii for the VoidFinder (left), V^2/VIDE (center), and V^2/REVOLVER (right) SDSS DR7 void catalogs (solid lines) generated assuming WMAP5 cosmology. The shaded uncertainties were computed using 64 DR7 mock catalogs produced from the Horizon Run 4 simulation (Kim et al. 2015). VoidFinder voids are more numerous and generally smaller due to how V^2 aggregates disconnected voids (see Section 4.3 for discussion). We extend the V^2/REVOLVER distribution down to 10 h^{-1} Mpc so that it is consistent with both VoidFinder and V^2/VIDE.

mock galaxy catalogs than in data. Likewise, we would expect the V^2 algorithm to find slightly more void galaxies and slightly smaller voids in the mock galaxy catalog than in data, since the voids will spread to smaller radii when the density gradient is more shallow but the linking density remains fixed. This is consistent with the mock void catalog properties summarized in Tables 6 and 7.

For all algorithms used, the density profiles display qualitative agreement with previous void studies, both on data (e.g., Pan et al. 2012; Ceccarelli et al. 2013; Nadathur & Hotchkiss 2014; Ricciardelli et al. 2014) and simulations (e.g., Colberg et al. 2008; Lavaux & Wandelt 2012; Hamaus et al. 2014a; Sutter et al. 2014a). In particular, void density profiles produced specifically from the SDSS DR7 such as those in Pan et al. (2012) and Sutter et al. (2012b) display a similar behavior at large r, where $1 + \delta$ levels off below 1 due to the relatively small size of the survey volume.

5. COMPARISON TO PREVIOUS VOID CATALOGS

Previous void catalogs based on SDSS DR7 have been created, including Pan et al. (2012) with VoidFinder, and Sutter et al. (2012b) and Nadathur & Hotchkiss (2014) with ZOBOV. Each of these void catalogs is based on a different volume-limited version of SDSS DR7, and each handles the survey boundaries differently. Our void catalogs address these issues and improve upon these earlier catalogs. Below, we focus on the improvements in our VoidFinder SDSS DR7 void catalog relative to earlier versions, as comparisons to all previously published void catalogs is beyond the scope of this work.

5.1. *Choice of galaxy catalog*

The VoidFinder void catalog described in Pan et al. (2012) is based on the Korea Institute for Advanced Study Value-Added Galaxy Catalog (KIAS-VAGC; Choi et al. 2010) and its main source the New York University Value-Added Galaxy Catalog (NYU-VAGC; Blanton et al. 2005). The volume-limited catalog used by Pan et al. (2012) requires galaxies to have $M_r < -20.09$ and $z < 0.107$, while we require $M_r < -20.0$ and $z < 0.114$. The redshift limit that we use is better matched to the maximum redshift at which a galaxy with $M_r = -20.0$ is observed in the magnitude-limited SDSS DR7 spectroscopic survey ($m_r < 17.77$).

We choose to use the NSA as our galaxy catalog for three main reasons. First, the KIAS-VAGC assigns a redshift to galaxies with $m_r < 17.77$ that were not spectroscopically targeted in SDSS DR7 due to their proximity with another spectroscopic target (avoiding fiber collisions). While it is sometimes a safe assumption that two galaxies with this small sky separation are actually close in redshift, some of these objects have since been spectroscopically observed and found to have a significantly different redshift than their projected nearest neighbor. Second, the NSA better handles large galaxies, preventing them from being segmented into a number of spurious small unique objects. Finally, the NSA also does not include galaxies close to bright stars, whose photometry might be affected by the star's light. All of these properties impact the volume-limited catalog used for void-finding, slightly affecting the voids found with the algorithms.

5.2. *Handling survey boundaries*

Relative to Pan et al. (2012), our implementation of VoidFinder improves on the handling of the survey boundaries and on the merging of smaller spheres into

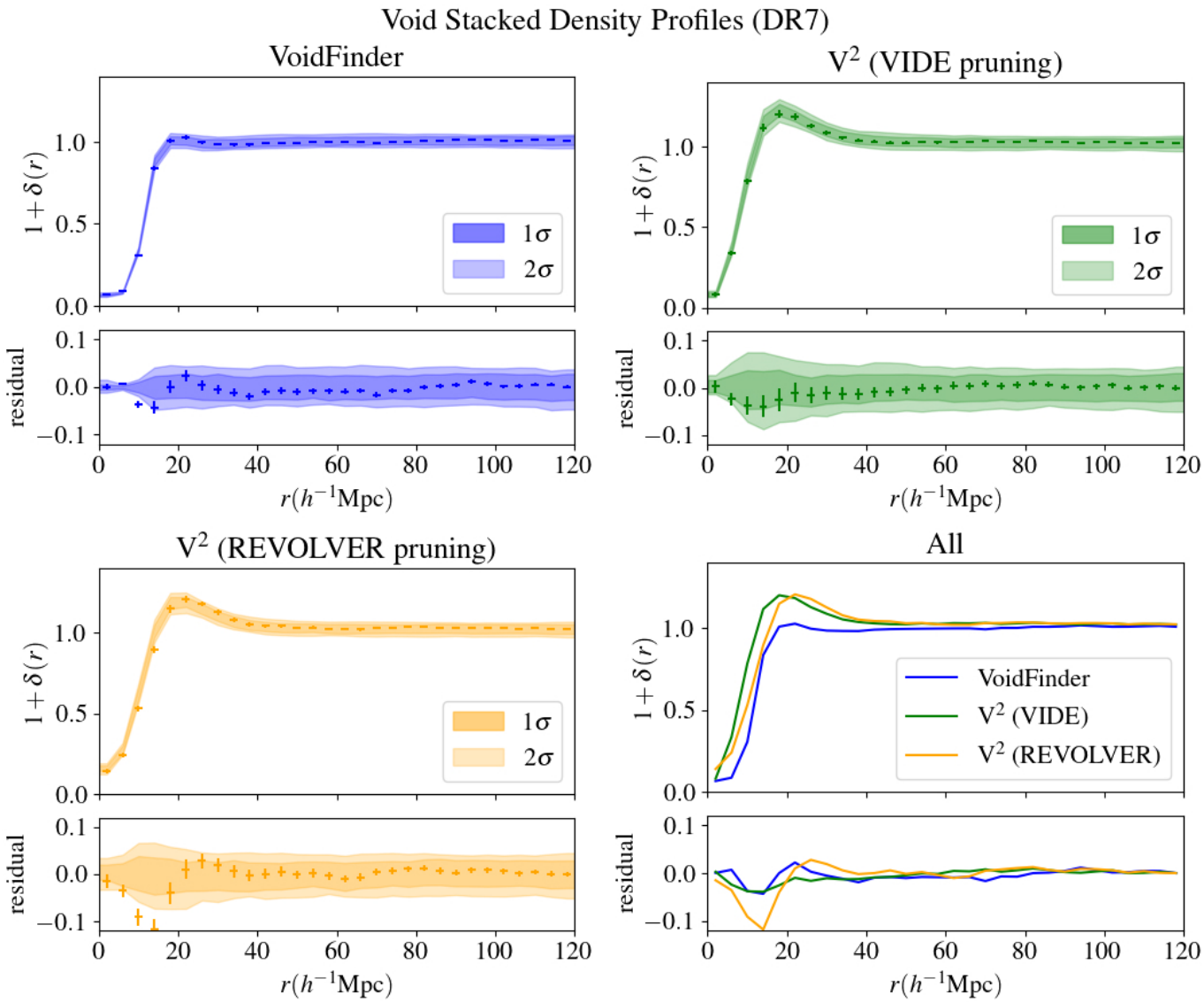


Figure 5. Stacked radial void density profiles, measured in concentric spherical shells around void centers generated assuming the WMAP5 cosmology. We estimate the profiles using the average density of all galaxies, measured from the centers of voids. $1 + \delta = 1$ corresponds to the mean survey density, while $1 + \delta = 0$ corresponds to a density of 0.

the voids. As seen in Figure 7, the void catalog from Pan et al. (2012) includes a large number of voids near the survey edge, resulting from the growth of spheres into the empty space beyond the survey limits. This is the source of the erroneous large voids included in the void catalog by Pan et al. (2012). As described in Section 3.1, we mitigate this effect by removing all spheres which extend beyond the survey bounds by more than 10% of their volume. Further, there is significant overlap between many of the voids, double-counting some of the survey volume and returning voids which are not dynamically distinct. Our implementation of VoidFinder avoids this by succinctly limiting the extent to which unique voids can overlap (see Section 3.1 for details).

Another way to handle survey boundaries is to populate the edges with an artificially high density of galaxies, thereby creating a dense wall through which no void will reach. In this manner, Sutter et al. (2012b) placed random particles along the survey boundaries to determine which galaxies' Voronoi cells should be assigned infinite density to prevent the growth of voids beyond the survey edges. However, the density of these randomly distributed particles is not high enough to constrain the Voronoi volumes of the real galaxies, causing the central densities of the voids along the boundaries to be lower than expected. Instead, as described in Section 3.2, V^2 sets the volume of any Voronoi cell with a vertex outside of the survey boundaries to zero, naturally limiting the

Table 6. Properties of void catalogs

	Cosmology	Algorithm	$N_{\rm void}$	median $R_{\rm eff}$ [h^{-1} Mpc]	maximum $R_{\rm eff}$ [h^{-1} Mpc]	% survey volume in voids	% galaxies in voids
Data	Planck 2018	VoidFinder	1163	15.5 ± 0.1	28.7	60.8	17.6
		V^2/VIDE	531	16.8 ± 0.5	53.1	68.1	64.4
		V^2/REVOLVER	518	19.4 ± 0.4	40.9	90.8	82.3
	WMAP5	VoidFinder	1184	15.6 ± 0.1	28.7	61.1	18.2
		V^2/VIDE	534	17.1 ± 0.5	53.3	63.0	64.8
		V^2/REVOLVER	518	19.5 ± 0.4	41.2	86.5	82.3
Simulations	WMAP5	VoidFinder	1283 ± 21	15.4 ± 0.1	29.3 ± 1.6	60.4 ± 0.7	18.2 ± 0.4
		V^2/VIDE	558 ± 25	16.7 ± 0.4	52.4 ± 8.7	66.6 ± 3.0	62.8 ± 2.6
		V^2/REVOLVER	545 ± 19	19.2 ± 0.4	41.1 ± 3.1	88.7 ± 0.5	80.4 ± 0.5

NOTE—Properties of void catalogs made from the SDSS DR7 (top) and 64 mock galaxy catalogs created from the Horizon Run 4 simulation (bottom). The volume-limited catalogs are made with a redshift cut of $z < 0.114$ and an absolute magnitude cut of $M_r < -20$. Edge voids are excluded from all properties except $N_{\rm void}$.

Table 7. Void overlap between catalogs

	Cosmology	Algorithms A	Algorithms B	% survey volume in voids ($A \cap B$)	% galaxies in voids ($A \cap B$)
Data	Planck 2018	VoidFinder	V^2/VIDE	40.9	11.0
		VoidFinder	V^2/REVOLVER	56.3	13.7
		V^2/VIDE	V^2/REVOLVER	63.3	58.3
	WMAP5	VoidFinder	V^2/VIDE	37.9	11.4
		VoidFinder	V^2/REVOLVER	51.8	14.1
		V^2/VIDE	V^2/REVOLVER	62.9	58.6
Simulations	WMAP5	VoidFinder	V^2/VIDE	40.0 ± 1.9	11.7 ± 0.5
		VoidFinder	V^2/REVOLVER	54.9 ± 0.8	15.7 ± 0.4
		V^2/VIDE	V^2/REVOLVER	62.0 ± 3.0	56.8 ± 2.6

NOTE—Percentage of overlap in survey volume and galaxies found in voids in the SDSS DR7 between each of the void catalogs. Edge voids are excluded from all percentages.

void growth along the survey edges without generating an artificial wall surrounding the survey.

5.3. *Consistent volume-limited galaxy catalog*

Void catalogs previously published for the SDSS DR7 using different void-finding algorithms used different cosmologies as well as different magnitude and redshift limits, making a direct comparison of the algorithms' results difficult. Our void catalogs are all created from the same volume-limited sample using a single cosmology and with similar void-finding parameters when possible (such as the minimum void radius). This allows for simple, direct comparison of the results from the various algorithms.

6. CONCLUSIONS

Using the SDSS DR7 NSA galaxy catalog, we have created a volume-limited catalog of 194,125 galaxies with $M_r < -20$ at $z < 0.114$. We use Python implementations of the VoidFinder (El-Ad & Piran 1997; Hoyle & Vogeley 2002) and ZOBOV (Neyrinck 2008) algorithms from the Void Analysis Software Toolkit (VAST; Douglass et al. 2022) to find voids in this volume-limited galaxy catalog. We also apply the same void-finding algorithms to 64 mock galaxy catalogs produced

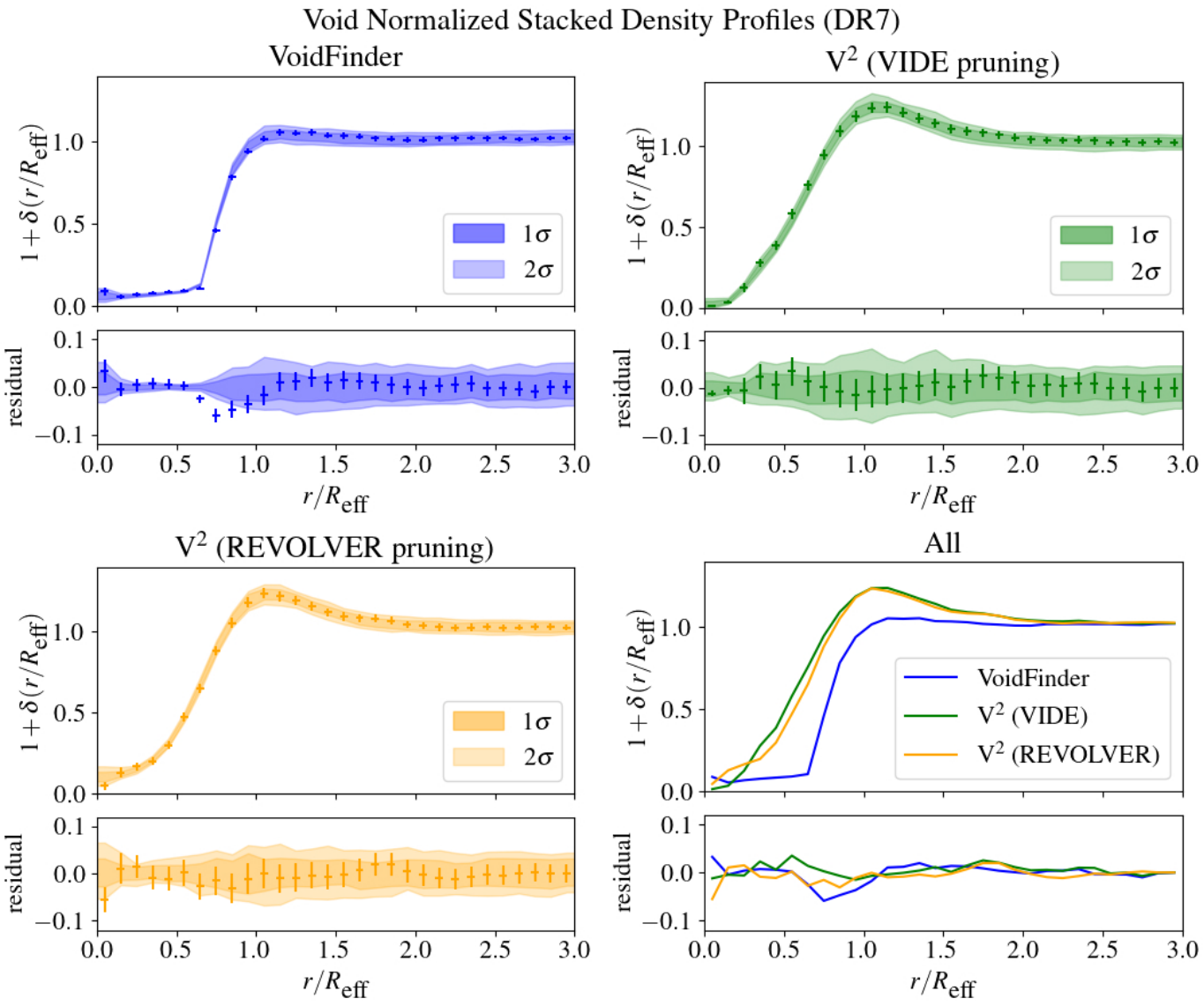


Figure 6. Stacked normalized radial void density profiles assuming WMAP5 cosmology, measured in concentric spherical shells around void centers. We estimate the profiles using the average density of all galaxies, measured from the centers of voids. The radii of the spherical shells are normalized to each void's effective radius, $R_{\rm eff}$. $1+\delta = 1$ corresponds to the mean survey density, while $1+\delta = 0$ corresponds to a density of 0.

from the Horizon Run 4 simulation (Kim et al. 2015). Three void catalogs based on VoidFinder, V^2/VIDE, and V^2/REVOLVER have been made public[4].

The computed properties of these void populations display good agreement between the data and mock catalogs, although V^2 tends to find fewer and larger voids than VoidFinder. This is especially true for V^2/VIDE and is a result of the linking of underdense "zones." Our findings qualitatively agree with other public void catalogs (Pan et al. 2012; Sutter et al. 2012b; Nadathur & Hotchkiss 2014), exhibiting a central underdensity in the stacked void profiles that is surrounded by an overdensity at $r \approx R_{\rm eff}$ in the normalized profiles.

Our void catalogs are suited for void-based studies in both cosmology and astrophysics. The positions of voids can be used in void-galaxy cross-correlations, in Alcock-Paczyński tests, in studies of CMB lensing by voids, and in studies of void ellipticities. Further, the identification of galaxies in voids can be used to study galactic properties in dense vs. underdense regions.

Both methods presented here come with particular advantages and disadvantages. The watershed technique (V^2) is simple and relatively free of tunable parameters, while VoidFinder requires the user to define sev-

[4] The catalogs are available in `ASCII` format at https://doi.org/10.5281/zenodo.5834786.

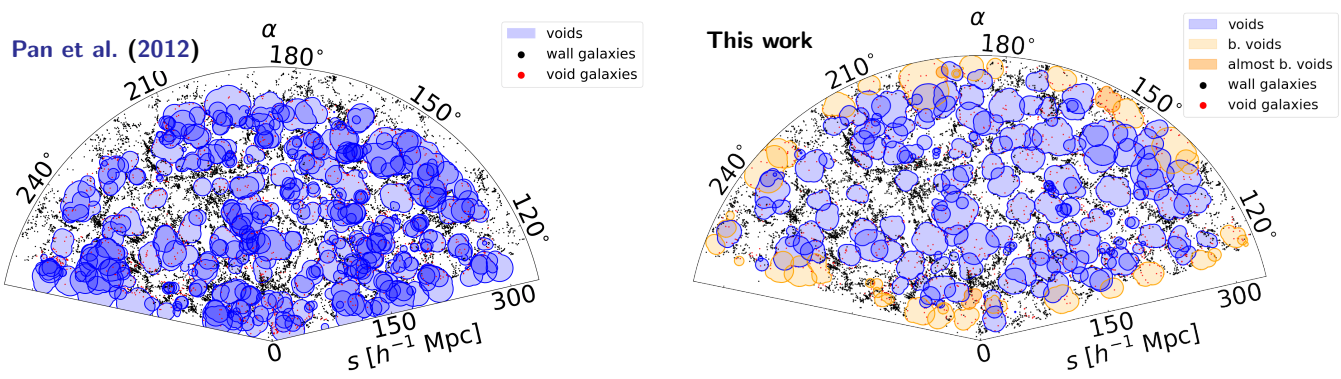


Figure 7. Same region of the SDSS DR7 survey, showing the intersection of the voids published by Pan et al. (2012) (left) and our VoidFinder catalog (right) generated assuming a Planck 2018 cosmology. The excess void regions identified by Pan et al. (2012) are easily seen along the boundaries of the survey. Within the footprint, we also see that the void catalog published by Pan et al. (2012) has significant overlap between identified voids.

eral parameters (e.g., void sphere overlap fraction and field galaxy criterion). We find that V^2 includes the shell-crossing regions as part of the void volume, while VoidFinder excludes them. The choice of which void catalog to use then depends on the intended science, since the dynamics in the shell-crossing regions around voids are significantly different than within the void interiors. As a result, the VoidFinder catalog is especially suited for studies of galaxy properties (Zaidouni et al., in prep). We find the extension of V^2 voids into overdense regions also leads to a very large fraction of galaxies classified as void. Similarly, our void catalogs can be used to study the properties of the intergalactic medium — for example, in searches for the prevalence of Lyman-α absorption in voids (Watson & Vogeley 2022).

ACKNOWLEDGEMENTS

The authors would like to thank Stephen W. O'Neill, Jr. for his help improving the VoidFinder algorithm in VAST, and Michael Vogeley and Fiona Hoyle for the original VoidFinder code and void-finding expertise. D.V. and S.B. acknowledge support from the U.S. Department of Energy Office of High Energy Physics under the grant DE-SC0008475. K.D. and D.V. acknowledge support from grant 62177 from the John Templeton Foundation.

The authors thank the Center for Integrated Research Computing (CIRC) at the University of Rochester for providing computational resources and technical support.

Funding for the SDSS and SDSS-II has been provided by the Alfred P. Sloan Foundation, the Participating Institutions, the National Science Foundation, the U.S. Department of Energy, the National Aeronautics and Space Administration, the Japanese Monbukagakusho, the Max Planck Society, and the Higher Education Funding Council for England. The SDSS web site is http://www.sdss.org/.

The SDSS is managed by the Astrophysical Research Consortium for the Participating Institutions. The Participating Institutions are the American Museum of Natural History, Astrophysical Institute Potsdam, University of Basel, University of Cambridge, Case Western Reserve University, University of Chicago, Drexel University, Fermilab, the Institute for Advanced Study, the Japan Participation Group, Johns Hopkins University, the Joint Institute for Nuclear Astrophysics, the Kavli Institute for Particle Astrophysics and Cosmology, the Korean Scientist Group, the Chinese Academy of Sciences (LAMOST), Los Alamos National Laboratory, the Max-Planck-Institute for Astronomy (MPIA), the Max-Planck-Institute for Astrophysics (MPA), New Mexico State University, Ohio State University, University of Pittsburgh, University of Portsmouth, Princeton University, the United States Naval Observatory, and the University of Washington.

REFERENCES

Abazajian, K. N., Adelman-McCarthy, J. K., Agüeros, M. A., et al. 2009, ApJS, 182, 543, doi: 10.1088/0067-0049/182/2/543

Alpaslan, M., Robotham, A. S. G., Obreschkow, D., et al. 2014, MNRAS, 440, L106, doi: 10.1093/mnrasl/slu019

Blanton, M. R., Kazin, E., Muna, D., Weaver, B. A., & Price-Whelan, A. 2011, AJ, 142, 31, doi: 10.1088/0004-6256/142/1/31

Blanton, M. R., Lin, H., Lupton, R. H., et al. 2003, AJ, 125, 2276, doi: 10.1086/344761

Blanton, M. R., Schlegel, D. J., Strauss, M. A., et al. 2005, AJ, 129, 2562, doi: 10.1086/429803

Bond, J. R., Kofman, L., & Pogosyan, D. 1996, Nature, 380, 603, doi: 10.1038/380603a0

Cai, Y.-C., Neyrinck, M. C., Szapudi, I., Cole, S., & Frenk, C. S. 2014, ApJ, 786, 110, doi: 10.1088/0004-637X/786/2/110

Ceccarelli, L., Paz, D., Lares, M., Padilla, N., & Lambas, D. G. 2013, MNRAS, 434, 1435, doi: 10.1093/mnras/stt1097

Chantavat, T., Sawangwit, U., & Wandelt, B. D. 2017, ApJ, 836, 156, doi: 10.3847/1538-4357/836/2/156

Chen, B., Kantowski, R., & Dai, X. 2015, ApJ, 804, 73, doi: 10.1088/0004-637X/804/1/73

Choi, Y.-Y., Han, D.-H., & Kim, S. S. 2010, Journal of Korean Astronomical Society, 43, 191, doi: 10.5303/JKAS.2010.43.6.191

Colberg, J. M., Pearce, F., Foster, C., et al. 2008, MNRAS, 387, 933, doi: 10.1111/j.1365-2966.2008.13307.x

Dai, D.-C. 2015, MNRAS, 454, 3590, doi: 10.1093/mnras/stv2208

de Lapparent, V., Geller, M. J., & Huchra, J. P. 1986, ApJL, 302, L1, doi: 10.1086/184625

Douglass, K. A., Smith, J. A., & Demina, R. 2019, ApJ, 886, 153, doi: 10.3847/1538-4357/ab4bce

Douglass, K. A., Veyrat, D., O'Neill, S. W., et al. 2022, Journal of Open Source Software, 7, 4033, doi: 10.21105/joss.04033

Douglass, K. A., & Vogeley, M. S. 2017a, ApJ, 834, 186, doi: 10.3847/1538-4357/834/2/186

—. 2017b, ApJ, 837, 42, doi: 10.3847/1538-4357/aa5e53

Douglass, K. A., Vogeley, M. S., & Cen, R. 2018, ApJ, 864, 144, doi: 10.3847/1538-4357/aad86e

Dunkley, J., Komatsu, E., Nolta, M. R., et al. 2009, ApJS, 180, 306, doi: 10.1088/0067-0049/180/2/306

El-Ad, H., & Piran, T. 1997, ApJ, 491, 421, doi: 10.1086/304973

Florez, J., Berlind, A. A., Kannappan, S. J., et al. 2021, ApJ, 906, 97, doi: 10.3847/1538-4357/abca9f

Fraser-McKelvie, A., Pimbblet, K. A., Penny, S. J., & Brown, M. J. I. 2016, MNRAS, 459, 754, doi: 10.1093/mnras/stw677

Fukugita, M., Ichikawa, T., Gunn, J. E., et al. 1996, AJ, 111, 1748, doi: 10.1086/117915

Furniss, A., Sutter, P. M., Primack, J. R., & Domínguez, A. 2015, MNRAS, 446, 2267, doi: 10.1093/mnras/stu2196

Geller, M. J., & Huchra, J. P. 1989, Science, 246, 897, doi: 10.1126/science.246.4932.897

Goh, T., Primack, J., Lee, C. T., et al. 2019, MNRAS, 483, 2101, doi: 10.1093/mnras/sty3153

Goldberg, D. M., & Vogeley, M. S. 2004, ApJ, 605, 1, doi: 10.1086/382143

Gregory, S. A., & Thompson, L. A. 1978, ApJ, 222, 784, doi: 10.1086/156198

Gunn, J. E., Carr, M., Rockosi, C., et al. 1998, AJ, 116, 3040, doi: 10.1086/300645

Habouzit, M., Pisani, A., Goulding, A., et al. 2020, MNRAS, 493, 899, doi: 10.1093/mnras/staa219

Hamaus, N., Pisani, A., Choi, J.-A., et al. 2020, JCAP, 2020, 023, doi: 10.1088/1475-7516/2020/12/023

Hamaus, N., Pisani, A., Sutter, P. M., et al. 2016, PhRvL, 117, 091302, doi: 10.1103/PhysRevLett.117.091302

Hamaus, N., Sutter, P. M., & Wandelt, B. D. 2014a, PhRvL, 112, 251302, doi: 10.1103/PhysRevLett.112.251302

Hamaus, N., Wandelt, B. D., Sutter, P. M., Lavaux, G., & Warren, M. S. 2014b, PhRvL, 112, 041304, doi: 10.1103/PhysRevLett.112.041304

Hong, S. E., Park, C., & Kim, J. 2016, ApJ, 823, 103, doi: 10.3847/0004-637X/823/2/103

Hoyle, F., & Vogeley, M. S. 2002, ApJ, 566, 641, doi: 10.1086/338340

Hoyle, F., Vogeley, M. S., & Pan, D. 2012, MNRAS, 426, 3041, doi: 10.1111/j.1365-2966.2012.21943.x

Huchra, J., Davis, M., Latham, D., & Tonry, J. 1983, ApJS, 52, 89, doi: 10.1086/190860

Ilić, S., Langer, M., & Douspis, M. 2013, A&A, 556, A51, doi: 10.1051/0004-6361/201321150

Jõeveer, M., Einasto, J., & Tago, E. 1978, MNRAS, 185, 357, doi: 10.1093/mnras/185.2.357

Jamieson, D., & Loverde, M. 2021, PhRvD, 103, 103522, doi: 10.1103/PhysRevD.103.103522

Kim, J., Park, C., L'Huillier, B., & Hong, S. E. 2015, Journal of Korean Astronomical Society, 48, 213, doi: 10.5303/JKAS.2015.48.4.213

Kirshner, R. P., Oemler, A., J., Schechter, P. L., & Shectman, S. A. 1981, ApJL, 248, L57, doi: 10.1086/183623

Kitaura, F.-S., Chuang, C.-H., Liang, Y., et al. 2016, PhRvL, 116, 171301, doi: 10.1103/PhysRevLett.116.171301

Lavaux, G., & Wandelt, B. D. 2012, ApJ, 754, 109, doi: 10.1088/0004-637X/754/2/109

Lee, J., & Hoyle, F. 2015, ApJ, 803, 45, doi: 10.1088/0004-637X/803/1/45
Liang, Y., Zhao, C., Chuang, C.-H., Kitaura, F.-S., & Tao, C. 2016, MNRAS, 459, 4020, doi: 10.1093/mnras/stw884
Liu, C.-X., Pan, D. C., Hao, L., et al. 2015, ApJ, 810, 165, doi: 10.1088/0004-637X/810/2/165
Lupton, R., Gunn, J. E., Ivezić, Z., Knapp, G. R., & Kent, S. 2001, in Astronomical Society of the Pacific Conference Series, Vol. 238, Astronomical Data Analysis Software and Systems X, ed. J. Harnden, F. R., F. A. Primini, & H. E. Payne, 269
Mao, Q., Berlind, A. A., Scherrer, R. J., et al. 2017, ApJ, 835, 160, doi: 10.3847/1538-4357/835/2/160
Melchior, P., Sutter, P. M., Sheldon, E. S., Krause, E., & Wandelt, B. D. 2014, MNRAS, 440, 2922, doi: 10.1093/mnras/stu456
Miraghaei, H. 2020, AJ, 160, 227, doi: 10.3847/1538-3881/abafb1
Moorman, C. M., Moreno, J., White, A., et al. 2016, ApJ, 831, 118, doi: 10.3847/0004-637X/831/2/118
Moorman, C. M., Vogeley, M. S., Hoyle, F., et al. 2014, MNRAS, 444, 3559, doi: 10.1093/mnras/stu1674
—. 2015, ApJ, 810, 108, doi: 10.1088/0004-637X/810/2/108
Nadathur, S., Carter, P. M., Percival, W. J., Winther, H. A., & Bautista, J. E. 2019, PhRvD, 100, 023504, doi: 10.1103/PhysRevD.100.023504
Nadathur, S., & Hotchkiss, S. 2014, MNRAS, 440, 1248, doi: 10.1093/mnras/stu349
Neyrinck, M. C. 2008, MNRAS, 386, 2101, doi: 10.1111/j.1365-2966.2008.13180.x
Pan, D. C., Vogeley, M. S., Hoyle, F., Choi, Y.-Y., & Park, C. 2012, MNRAS, 421, 926, doi: 10.1111/j.1365-2966.2011.20197.x
Paranjape, A., & Alam, S. 2020, MNRAS, 495, 3233, doi: 10.1093/mnras/staa1379
Penny, S. J., Brown, M. J. I., Pimbblet, K. A., et al. 2015, MNRAS, 453, 3519, doi: 10.1093/mnras/stv1926
Pisani, A., Lavaux, G., Sutter, P. M., & Wandelt, B. D. 2014, MNRAS, 443, 3238, doi: 10.1093/mnras/stu1399
Pisani, A., Sutter, P. M., Hamaus, N., et al. 2015, PhRvD, 92, 083531, doi: 10.1103/PhysRevD.92.083531
Planck Collaboration, Ade, P. A. R., Aghanim, N., et al. 2014, A&A, 571, A19, doi: 10.1051/0004-6361/201321526
Planck Collaboration, Aghanim, N., Akrami, Y., et al. 2020, A&A, 641, A6, doi: 10.1051/0004-6361/201833910
Ricciardelli, E., Quilis, V., & Varela, J. 2014, MNRAS, 440, 601, doi: 10.1093/mnras/stu307
Rood, H. J. 1988, ARA&A, 26, 245, doi: 10.1146/annurev.aa.26.090188.001333
Sheth, R. K., & van de Weygaert, R. 2004, MNRAS, 350, 517, doi: 10.1111/j.1365-2966.2004.07661.x
Shim, J., Lee, J., & Hoyle, F. 2015, ApJ, 815, 107, doi: 10.1088/0004-637X/815/2/107
Strauss, M. A., Weinberg, D. H., Lupton, R. H., et al. 2002, AJ, 124, 1810, doi: 10.1086/342343
Sutter, P. M., Lavaux, G., Hamaus, N., et al. 2014a, MNRAS, 442, 462, doi: 10.1093/mnras/stu893
Sutter, P. M., Lavaux, G., Wandelt, B. D., & Weinberg, D. H. 2012a, ApJ, 761, 187, doi: 10.1088/0004-637X/761/2/187
—. 2012b, ApJ, 761, 44, doi: 10.1088/0004-637X/761/1/44
Sutter, P. M., Pisani, A., Wandelt, B. D., & Weinberg, D. H. 2014b, MNRAS, 443, 2983, doi: 10.1093/mnras/stu1392
Sutter, P. M., Lavaux, G., Hamaus, N., et al. 2015, Astronomy and Computing, 9, 1, doi: 10.1016/j.ascom.2014.10.002
Tejos, N., Morris, S. L., Crighton, N. H. M., et al. 2012, MNRAS, 425, 245, doi: 10.1111/j.1365-2966.2012.21448.x
Trevisan, M., Mamon, G. A., Thuan, T. X., et al. 2021, MNRAS, 502, 4815, doi: 10.1093/mnras/staa4008
van de Weygaert, R., & Platen, E. 2011, in International Journal of Modern Physics Conference Series, Vol. 1, International Journal of Modern Physics Conference Series, 41–66, doi: 10.1142/S2010194511000092
Verza, G., Pisani, A., Carbone, C., Hamaus, N., & Guzzo, L. 2019, JCAP, 2019, 040, doi: 10.1088/1475-7516/2019/12/040
Watson, W. E., & Vogeley, M. S. 2022, arXiv e-prints, arXiv:2204.06708. https://arxiv.org/abs/2204.06708
Zhao, C., Chuang, C.-H., Kitaura, F.-S., et al. 2020, MNRAS, 491, 4554, doi: 10.1093/mnras/stz3339
Zhao, C., Variu, A., He, M., et al. 2021, arXiv e-prints, arXiv:2110.03824. https://arxiv.org/abs/2110.03824